1 Introduction

This book deals with structures, fixed or floating, in the open sea, unprotected or ill-protected from the environment, at fixed locations: Forward speed effects (i.e., ships under sailing conditions) are not considered. One of the main applications considered is the design of the supports used for oil exploration and exploitation (Figure 1.1). Many of them are represented in the accompanying figures. As the figures show these structures come in a wide variety of geometries and sizes. Reference will often be made to the following supports:

- *Jacket* (Figure 1.2): a fixed platform, nailed to the sea floor, consisting in an assembly of tubular members. Jackets are used for oil production in water depths up to 200 m (roughly) and also as supports for wind turbines.
- *Jack-up* or self-elevating unit: consisting in a buoyant hull and three or four movable legs, capable of raising the hull above the sea surface. Jack-ups are used for drilling at shallow depths. They are also widely used for work at sea, for instance, for installation of the hubs and blades of wind turbines.
- Gravity base structure (GBS): in concrete, resting on the seabed, also used for oil and gas production (Figure 1.3) or liquefied natural gas (LNG) storage. Small size GBSs are nowadays used as supports for offshore wind turbines, for instance, in the English Channel, off the coast of Normandy (Fécamp wind farm).
- *Floating production storage offloading* (FPSO): floating support used for oil production, usually shipshaped and moored via a *turret* around which they can freely rotate (Figure 1.4) or, in mild areas, anchored with a spread mooring (Figure 1.5).
- *Floating liquefied natural gas* (FLNG): similar to FPSO but used for gas production, with the liquefaction plant onboard. The Prelude FLNG (Figure 6.41), off the western coast of Australia, is the largest man-made floating structure, with a displacement of 600,000 tons.
- semi-submersible platform (*semi*): usually comprising an assembly of four *columns* piercing the free surface and two horizontal *pontoons*. Semis are used for drilling, occasionally for production or as *floatels*, and as supports for wind turbines (Figure 1.6).
- *Tension leg platform* (TLP): similar to the semis but in excess of buoyancy, anchored vertically by *tethers* (Figure 1.7). The vertical motions are thus

https://doi.org/10.1017/9781009198059.003 Published online by Cambridge University Press

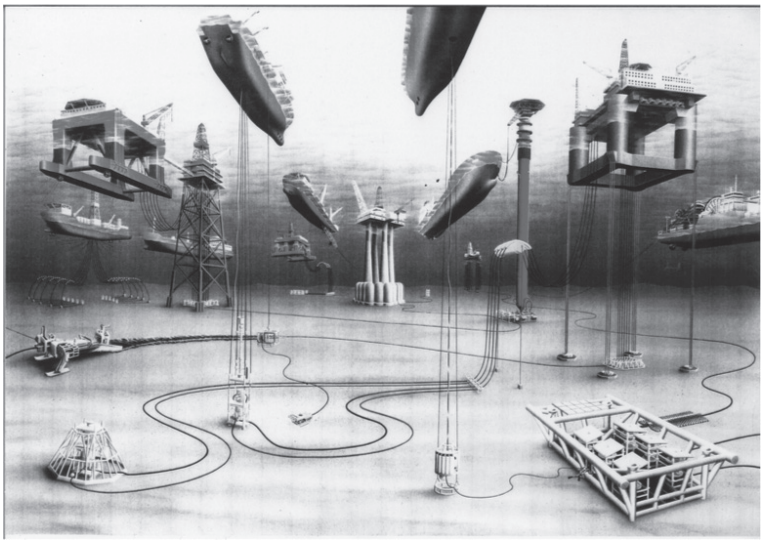

Figure 1.1 Offshore production systems (from Oilfield Publications Limited).

Figure 1.2 Bullwinkle jacket under tow (picture by Lanmon Aerial Photography, courtesy of Shell Exploration & Production Company).

suppressed, allowing location of the wellheads on the deck. TLPs are also used to support wind turbines (see Figure 1.8);

- Spar: truncated vertical cylinder of large draft, also used to support wind turbines.

Offshore oil is not the sole field of application considered here. Recent years have seen the rapid development of wind energy at sea, with the turbines first installed on fixed foundations and now on floating supports. The recovery of wave energy has been a long-standing research topic; even though the technology has not yet reached

https://doi.org/10.1017/9781009198059.003 Published online by Cambridge University Press

Figure 1.3 The Troll GBS under tow (courtesy Equinor).

the economically viable stage, active research is still going on. There are many other operations taking place in the open sea, such as deep-sea mining, laying telephone cables, or oceanographic exploration. Fish farming is another marine activity gradually moving into deeper and less-sheltered areas (Figure 1.9).

To design structures intended to operate at a given location over many years, a precise knowledge of the prevailing sea conditions is required, not only of the most extreme waves, wind, and current conditions but also of the daily sea states that cause fatigue. In areas such as the North Sea, where extreme wave heights can reach 30 m, waves are the dominant loading factor: They exert cyclic loads that the structures and foundations must withstand. Floating and elastic structures respond dynamically to the wave loads. All these wave-induced stresses and responses need to be evaluated at the design stage. Currents also exert loads on the floaters and on their connections to the sea floor with a possible dynamic response due to alternate vortex shedding.

https://doi.org/10.1017/9781009198059.003 Published online by Cambridge University Press

Figure 1.4 The Norne FPSO in the North Sea (courtesy Equinor).

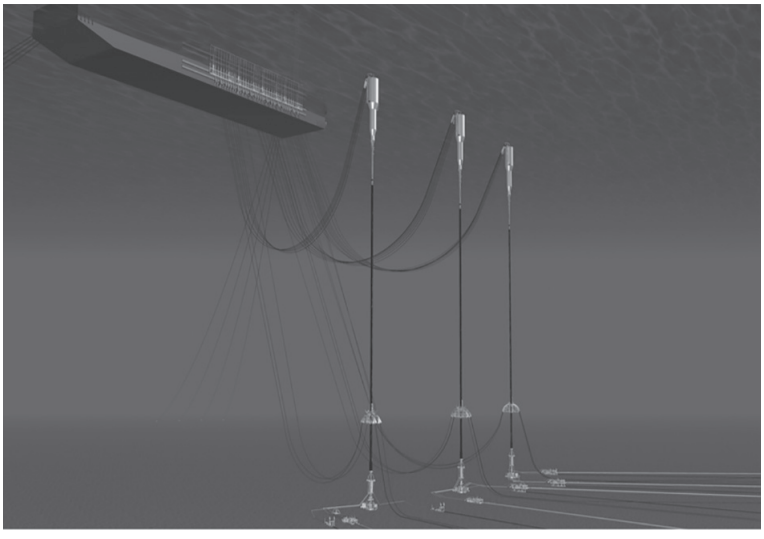

Figure 1.5 The Girassol FPSO off the coast of Angola and its riser towers (courtesy Doris Engineering).

https://doi.org/10.1017/9781009198059.003 Published online by Cambridge University Press

Figure 1.6 The floating wind turbine Windfloat 1 during construction in Portugal. Note the heave plates whose function is to increase the vertical added mass, shifting the heave and pitch natural periods out of the wave period range. Additional benefit comes from decreased wave excitation loads and increased viscous damping (courtesy Principle Power, Inc.).

Model testing, covered in Chapter 9, is a route to assess the wave and current responses of offshore structures. Due to the requirements of offshore oil developments, theoretical and numerical analyses have made huge progress over the past 50 years. The main purpose of this book is to provide a state-of-the-art survey of present knowledge and of the numerical tools available to offshore engineers.

Given the wide variety of the considered structures, some kind of classification is required. This is proposed in the following section, with criteria based first on their geometry and then on their types of wave responses.

1.1 Classification of Offshore Structures

1.1.1 Large or Small Bodies

Among the constitutive elements of offshore structures, there is a fairly recurrent geometrical form: the circular cylinder. Circular cylinders come in a wide range of

https://doi.org/10.1017/9781009198059.003 Published online by Cambridge University Press

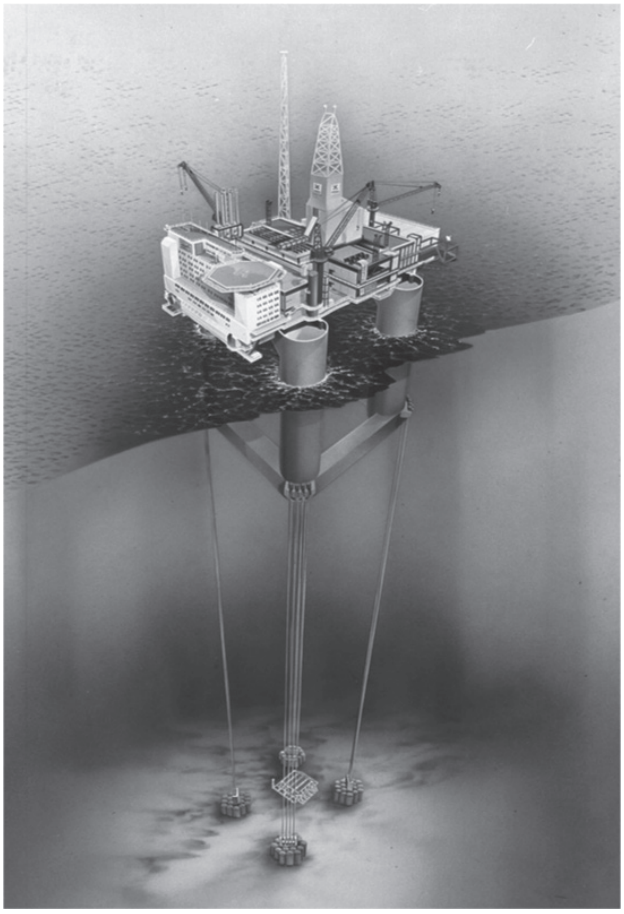

Figure 1.7 The Heidrun Tension Leg Platform in the North Sea (courtesy Equinor).

diameters: a few centimeters in the case of umbilicals and mooring lines, around a meter for the risers and jacket bars, 10 to 30 m for the columns of semi-submersible platforms and TLPs.

These cylindrical elements are subjected to the flow induced by waves and currents.

A circular cylinder is poorly streamlined: When subjected to current alone massive separation occurs (see Figure 1.10). Whether the boundary layers are laminar or turbulent, and where they separate, depends on the Reynolds number $\mathrm{Re} = U_C\, D/\nu$, where U_C is the current velocity, D the diameter, and ν the kinematic viscosity, $\nu \simeq 10^{-6}\ \mathrm{m^2\ s^{-1}}$ for sea water. Typically $U_C \sim 1$ m/s; therefore, the Reynolds numbers that we are concerned with range from 10^4 for cables and umbilicals 10 mm in diameter up to 10^7 for 10 m columns of semi-submersibles. It will be seen in Chapter 4 that it is for Reynolds numbers around 10^5 that the flow is the most intricate, with transition from laminar to turbulent taking place near the separation point.

In spite of its geometric simplicity, numerical modeling of a steady uniform flow around a circular cylinder at high Reynolds numbers (larger than 10^5) is still a challenge.

https://doi.org/10.1017/9781009198059.003 Published online by Cambridge University Press

Figure 1.8 The wind turbine floater developed by SBM Offshore, to be installed at the Provence Grand Large site, off the Gulf of Fos near Marseille (courtesy SBM Offshore).

Wave-induced flow differs fundamentally from current, in that it reverses periodically as the waves pass by. If one considers a vertical pile subjected to a regular wave, and if we isolate a slice of this pile, the situation presents a strong similarity to the two-dimensional problem of a cylinder in uniform oscillatory flow of velocity $A\,\omega\,\cos\omega t$. Experiments show that a fundamental parameter is the ratio A/D of the amplitude of flow motion A to the diameter D.

When the amplitude A is large compared to the diameter D, the flow has a strong similarity to the steady current case: At each half cycle, a wake is emitted and carried far away. The difference is that, when the flow reverses, the wake travels back to the cylinder, meaning incoming vorticity and turbulence. Conversely, when the ratio A/D is small, the fluid particles at the cylinder wall do not travel a long enough distance for the boundary layer to separate (see Figure 1.11). The thickness of the boundary layer,

https://doi.org/10.1017/9781009198059.003 Published online by Cambridge University Press

Figure 1.9 Dry transport of the Havfarm fish farm "Jostein Albert" (photo: Nordlaks/Deadline Media).

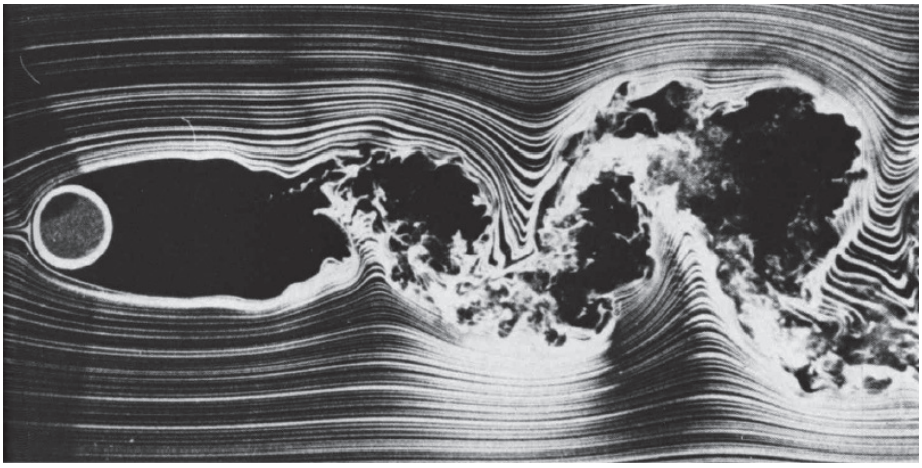

Figure 1.10 Uniform flow over a circular cylinder. Re = 10,000 (from van Dyke, 1982. Photograph by Thomas Corke and Hassan Nagib).

in laminar flow, is of the order $\sqrt{\nu/\omega}$, that is, for wave periods $T = 2\pi/\omega$ in-between 5 s and 20 s, 1 to 2 mm, quite negligible compared to the diameter in most cases. The outer flow is then adequately modeled by potential flow theory, that is, assuming perfect fluid and irrotationality, the streamlines being the same whether the flow is from left to right or right to left (Figure 1.12).

In place of the ratio A/D, the Keulegan–Carpenter number $\mathrm{K_C}$ defined as $\mathrm{K_C} = A\,\omega\,T/D = 2\,\pi A/D$ is usually taken as the discriminating parameter. The boundary between attached flow and separated flow depends on the $\mathrm{K_C}$ value, but also on the Reynolds number or, equivalently, on the Stokes parameter $\beta = \mathrm{Re}/\mathrm{K_C} = D^2/(\nu\,T)$.

https://doi.org/10.1017/9781009198059.003 Published online by Cambridge University Press

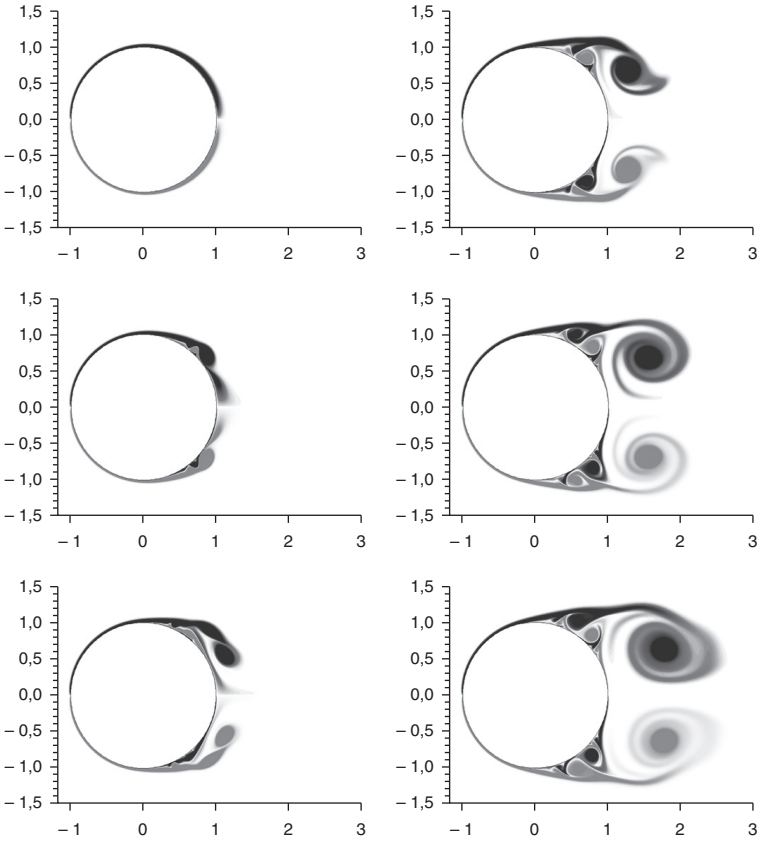

Figure 1.11 Navier–Stokes calculations at Re = 9,500 (from S. Etienne, 1999). The fluid is at rest and the flow starts impulsively at $t = 0$. The successive plots show the vorticity at times $U_C\, t/D$ going from 0.5 to 3. The boundary layer separates when the incoming flow has traveled between 0.5 and 1 diameter.

When the Stokes parameter is larger than about 10^5 (meaning a diameter larger than 1 m), separation does not occur until K_C exceeds 4 or 5. Referring to a semicolumn with a 20 m diameter, $K_C = 5$ means a wave amplitude around 15 m, close to the design wave in the North Sea!

It appears therefore legitimate to tackle the wave interaction with massive structures within the frame of a theory that assumes perfect fluid and irrotational flow: the potential flow theory. The characteristic dimensions of these "large bodies" are comparable to the wave lengths. As a result, when they interact with the structure, the incoming waves are significantly altered: they are "diffracted." When the structure responds to the waves, due to its motion another wave system is emitted, or "radiated." By means of some simplifying assumptions, potential flow theory offers the possibility to solve these diffraction and radiation problems, and to derive wave loads and responses.

In the absence of the body, it is also potential flow theory, which is used to describe the kinematics of the incoming waves.

https://doi.org/10.1017/9781009198059.003 Published online by Cambridge University Press

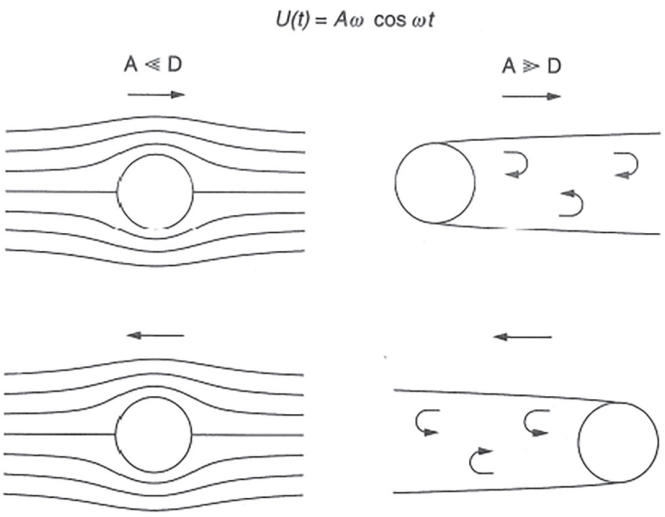

Figure 1.12 Oscillating flow around a circular cylinder. Limiting cases $A \ll D$ (left) and $A \gg D$ (right).

It is worth noting that, when a steady current coexists with an oscillatory flow, and the Keulegan–Carpenter number is low, the flow does not separate as long as the current velocity U_C is lower than the amplitude $A\,\omega$ of the oscillatory velocity. Potential flow theory is therefore applicable to the joint wave and current interaction with a large body, as long as the current velocity is smaller than the orbital velocities.

In contrast to large bodies, "small bodies" have characteristic dimensions smaller than or comparable to the amplitude of the fluid motion. They are therefore small compared to the wave lengths, with the result that diffraction effects are limited and that, locally, in the vicinity of a jacket bar slice, for example, the incident flow can be considered as uniform. The drawback is that the flow separates: Potential flow theory can no longer be applied; other numerical tools are required that solve the Navier–Stokes equations. The state-of-the-art is not to do Computational Fluid Dynamics (CFD) computations, but to relate, somewhat empirically, the local loads to the acceleration and velocity of the local incident flow, via the famous Morison formula. The inertia and drag coefficients that occur in this formulation are derived from representative tests.

The paradox is that the Morison equation, despite its imperfections, enables one to take into account a much more "refined" incident flow than the diffraction-radiation theory, limited to Stokes wave theories at first and second orders: The calculation of the hydrodynamic loading on jackets is usually done using third- or fifth-order Stokes theory or the stream function model.

It should not be concluded from the above that a given structure belongs to one of two categories. It can be both a large body and a small body, its constituent elements belonging to the two categories (the truss spars by example); it can be a small body under certain wave conditions and a large body in others (semi-submersibles).

https://doi.org/10.1017/9781009198059.003 Published online by Cambridge University Press

1.1.2 Types of Loadings and Responses

Energetic wave periods cover a range going roughly from 3 to 20 s. At these periods (more especially in the range of 8–16 s), the waves exert high loads on floating (or deformable) structures, inducing responses at the same periods, and with amplitudes more or less linearly related to the wave amplitude. Catastrophic responses can result in cases of resonance.

A technique often used to limit this type of response is to shift the natural periods out of the range of the wave periods. This is one reason to employ soft moorings: The natural periods in surge, sway, and yaw of floating structures are typically higher than a minute. Likewise, semisubmersibles platforms are designed in such a way that their natural periods in heave, roll, and pitch be above the local wave periods. Conversely, tension leg platforms have very stiff vertical moorings, and natural periods in heave, roll, and pitch of usually less than 3 or 4 s.

It would be naive to believe that such a strategy eliminates all risks of resonance. Practically, one always observes some response at the natural periods, no matter how far they are from the wave periods. Nonlinear mechanisms are the underlying cause of these responses, which can be of very high amplitudes when the associated damping ratios are low.

The most well-known of these nonlinear mechanisms results from extending to "second order" wave loading. In irregular waves, when the free surface elevation is written as

$$\eta_I(x,y,t) = \sum_i A_i \ \cos(k_i\, x\, \cos\beta + k_i\, y\, \sin\beta - \omega_i\, t + \theta_i) \tag{1.1}$$

(with $A_i^2 = 2\, S(\omega_i)\, \Delta\omega$, $S(\omega)$ being the wave spectrum),
the linear, or first-order, loads are obtained as:

$$F^{(1)}(t) = \Re\left\{\sum_i A_i\ f^{(1)}(\omega_i,\beta)\ \mathrm{e}^{-\mathrm{i}\,\omega_i\, t + \mathrm{i}\,\theta_i}\right\} \tag{1.2}$$

Equivalently, in the frequency domain:

$$S_{F^{(1)}}(\omega) = S(\omega)\ \|f^{(1)}(\omega,\beta)\|^2 \tag{1.3}$$

$f^{(1)}(\omega,\beta)$ being the complex transfer function, or RAO (Response Amplitude Operator). The free surface elevation and the linear loading cover the same range of frequencies.

Proceeding to second order, supplementary loads are obtained that take place at the sums and differences of the carrier frequencies:

- difference frequency component:

$$F_-^{(2)}(t) = \Re\left\{\sum_i \sum_j A_i\ A_j\ f_-^{(2)}(\omega_i,\omega_j,\beta)\ \mathrm{e}^{\mathrm{i}\,[-(\omega_i-\omega_j)\,t+\theta_i-\theta_j]}\right\} \tag{1.4}$$

https://doi.org/10.1017/9781009198059.003 Published online by Cambridge University Press

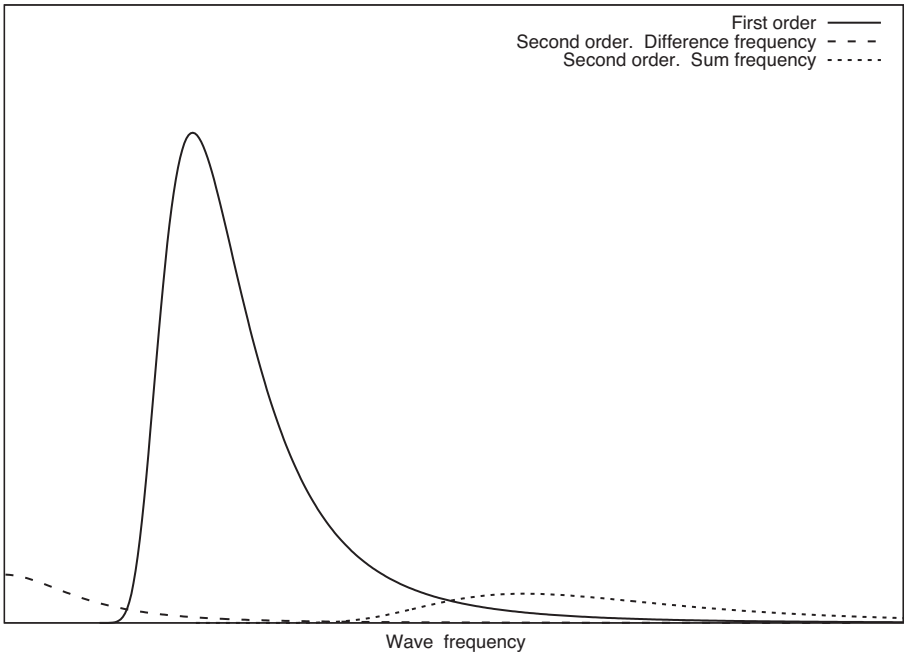

Figure 1.13 Spectra of the first- and second-order loads.

- sum frequency component:

$$F_+^{(2)}(t) = \Re\left\{\sum_i \sum_j A_i\ A_j\ f_+^{(2)}(\omega_i,\omega_j,\beta)\ \mathrm{e}^{\mathrm{i}\,[-(\omega_i+\omega_j)\,t+\theta_i+\theta_j]}\right\} \tag{1.5}$$

The complex quantities $f_-^{(2)}$ and $f_+^{(2)}$ are known as **Quadratic Transfer Functions** (QTFs). In the frequency domain the spectra of the second-order loads take the forms:

$$S_{F_-^{(2)}}(\Omega) = 8\ \int_0^\infty S(\omega)\ S(\omega+\Omega)\ \|f_-^{(2)}(\omega,\omega+\Omega,\beta)\|^2\ \mathrm{d}\omega \tag{1.6}$$

$$S_{F_+^{(2)}}(\Omega) = 8\ \int_0^{\Omega/2} S(\omega)\ S(\Omega-\omega)\ \|f_+^{(2)}(\omega,\Omega-\omega,\beta)\|^2\ \mathrm{d}\omega \tag{1.7}$$

A qualitative illustration is provided by Figure 1.13, which shows typical shapes of $S_{F^{(1)}}$, $S_{F_-^{(2)}}$, and $S_{F_+^{(2)}}$ vs the frequency ω. It can be seen that $S_{F_-^{(2)}}$ covers the complete low-frequency domain, from $\omega = 0$ up to the wave frequencies. The second-order difference frequency loads actually are a first approximation of the low-frequency part of the nonlinear wave loads. In a similar way, $S_{F_+^{(2)}}$ covers a large part of the high-frequency range, beyond the wave frequencies.

As their names suggest, these second-order loads are much lower in magnitude than the first-order loads. But they can lead to very large responses, in resonant conditions. This is the case of the horizontal movements of moored structures that typically have natural periods longer than one minute. At such periods linear theory provides no excitation; but the second-order of approximation yields low-frequency loads,

https://doi.org/10.1017/9781009198059.003 Published online by Cambridge University Press

Figure 1.14 The Eiko Maru storage tanker in the Arabian Gulf (from Molin & Bureau, 1980).

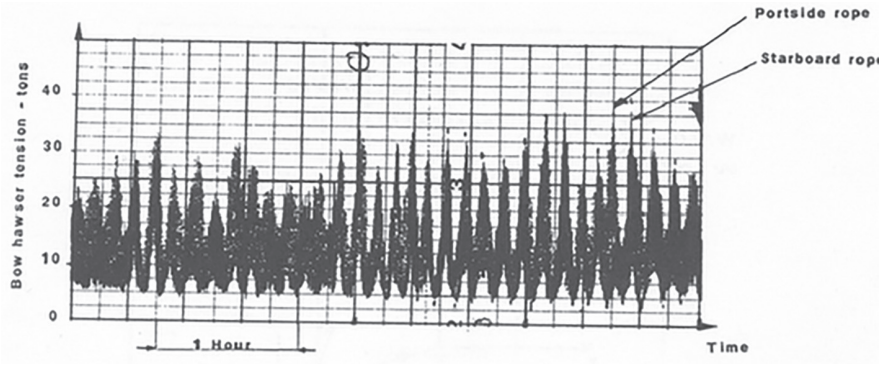

Figure 1.15 Eiko Maru tanker. Tension records in the bow hawsers (from Molin & Bureau, 1980).

so-called slowly-varying drift forces, that fluctuate in time roughly following the wave envelope signal.

Despite the fact that the loads are much weaker, the resulting slow-drift motions are much greater in amplitude than the first-order responses. Illustrations are provided in the following figures:

Figure 1.14 shows the storage tanker Eiko Maru in the Arabian Gulf. Figure 1.15 is a record of the bow hawsers tensions obtained by TotalEnergies in the late seventies. The dominant period in the record is close to 400 s, which is easily found to coincide with the natural period in surge, accounting for the combined stiffnesses of the hawsers and buoy anchoring (Molin & Bureau, 1980).

Figure 1.16 shows experimental records from tests, at Cehipar, on a large rectangular barge model (5 m long). Having their resonant frequencies in the wave frequency range, the time traces of the heave and roll responses look very similar to the wave elevation, whereas the sway motion is dominated by its slow-drift component, at its natural frequency.

https://doi.org/10.1017/9781009198059.003 Published online by Cambridge University Press

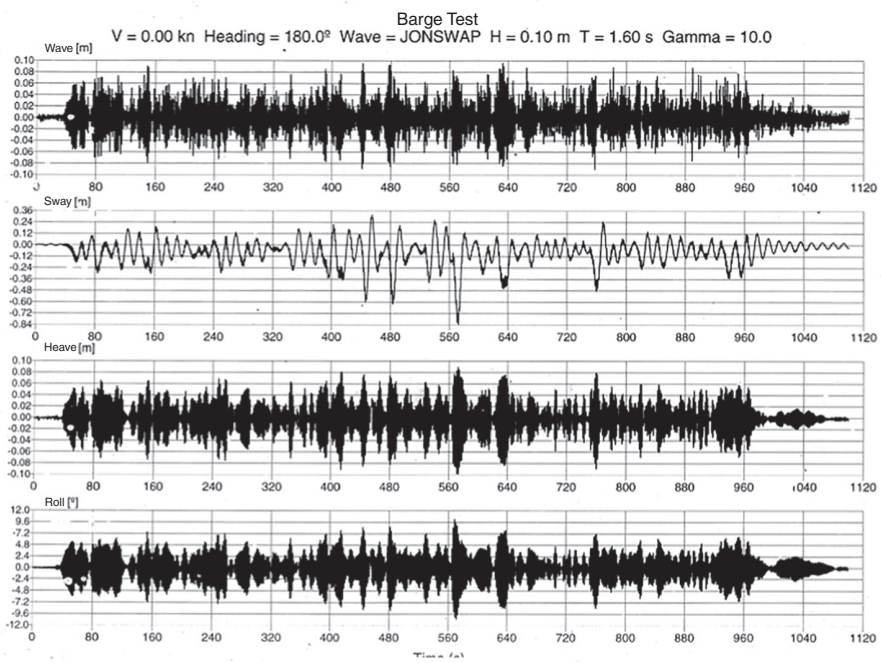

Figure 1.16 Model tests on a rectangular barge model in irregular beam waves. Time traces of the free surface elevation (top), sway, heave, and roll (bottom) motions.

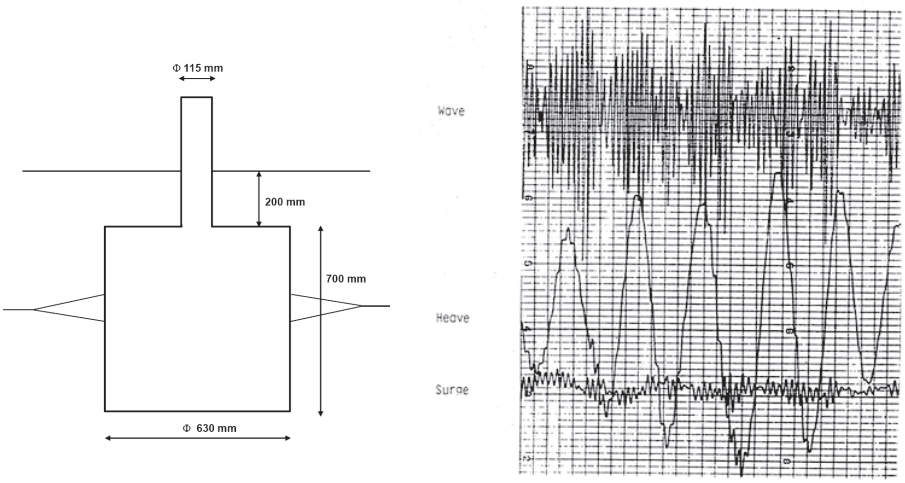

Figure 1.17 Model tests on a bottle-shaped model. Time traces of the free surface elevation (top), heave, and surge (bottom) motions.

Slow-drift motion may also occur for the vertical degrees of freedom, heave, roll, and pitch, when their natural frequencies are below the wave frequency range. Figure 1.17 shows experimental records of the heave and surge responses of a bottle-shaped

https://doi.org/10.1017/9781009198059.003 Published online by Cambridge University Press

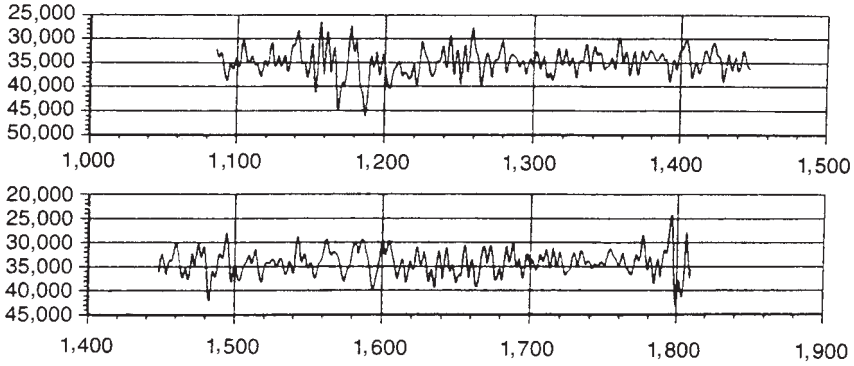

Figure 1.18 Model tests on a tension leg platform (PLTB 1,000). Time series of the tension in a tether.

model, where the low-frequency component of the heave response by far exceeds the wave frequency response.

The sum frequency second-order loads are considered responsible for the **springing**[1] behavior of Tension Leg Platforms, in sea states having peak periods around twice the heave, roll, and pitch natural periods. An example is shown in Figure 1.18 where tension fluctuations can be seen at a period of 5 s, when the peak period of the wave spectrum is 11 s. These experimental results are from an early TLP design, rather optimistic. Most existing TLPS have their natural periods somewhat lower, in the range 2–4 s. With these stiffer moorings, vibratory responses, known as **ringing**,[2] may still be observed in sea states having peak periods 4, 5, or 6 times larger than the natural periods, due to higher than second-order nonlinear wave loads. The ringing behavior was first discovered during the model tests undertaken for the Heidrun TLP and it was subsequently established that it is also a concern for deep water GBSs.

An example of ringing response is provided in Figure 1.20, which shows the effect of a steep wave group passing by an idealized GBS, a vertical cylinder, shown in Figure 1.19. The cylinder is connected to its foundation via an elastic steel plate, yielding a natural period of 0.44 s for the bending mode. The wave group has a mean period around 2 s; as it interacts with the cylinder, the third wave in the group, steeper and higher than the previous ones, triggers a vibratory response at the bending frequency.

With TLPs, springing is a concern to the fatigue life of the tethers, while ringing must be accounted for in design conditions. Obviously, to predict ringing numerically a second-order theory is insufficient when the ratio between resonant frequency and wave frequency is so wide. A third-order theory would exhibit loads taking place at frequencies $\omega_i + \omega_j + \omega_k$, probably still below the target frequency range.

It should be noted that other nonlinear phenomena, parametric instabilities, for instance, can induce resonant responses at frequencies different from the wave

[1] The coining springing was originally introduced to describe an elastic response of ship hulls.
[2] Another type of vibratory response of ship hulls.

https://doi.org/10.1017/9781009198059.003 Published online by Cambridge University Press

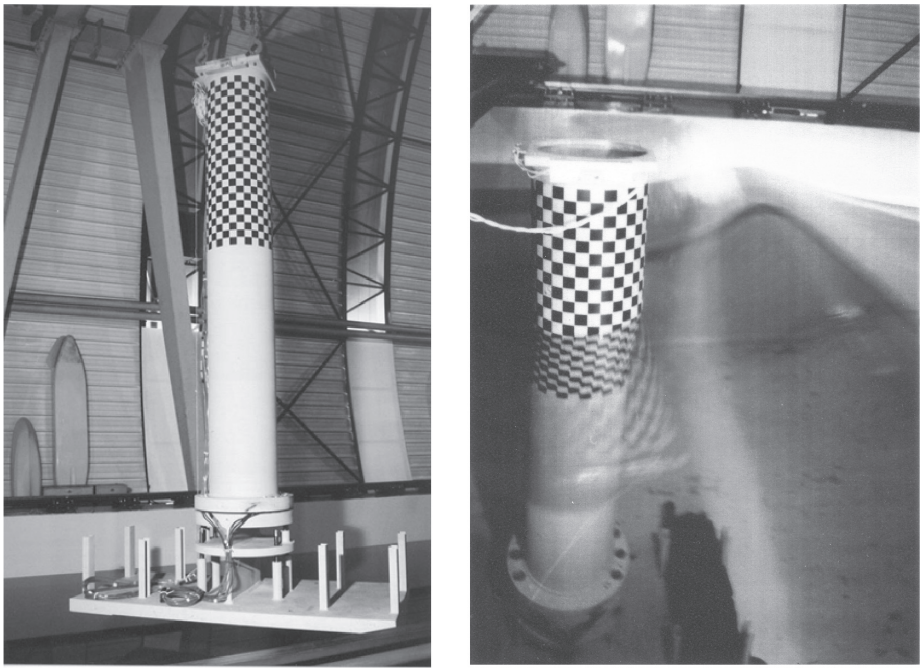

Figure 1.19 Model tests on a vibrating cylinder.

frequencies. A well-known case for ships is parametric roll that may occur when the wave encounter frequency is twice the roll natural frequency.

The determination, or at least the estimate, of its natural frequencies, is an important prerequisite in the hydrodynamic analysis of a system. It is also useful to have a proper estimate of the associated damping ratios.

1.2 Book Outline

The contents of this book are organized as follows:

Chapter 2 deals with environmental conditions. The main environmental factors are the waves (as measured, for instance, with a waverider buoy), the wind, and the current. The sea state concept is introduced, together with short-term and long-term statistics. The basic sea state parameters, that is, the significant wave height, mean wave periods, wave spectra, mean wind speeds, etc., are presented.

Chapter 3 presents the wave theories used in offshore engineering. Relatively deep water is assumed, so shallow water wave theories, such as cnoidal or solitary waves, are not covered. The classical Stokes perturbation method is introduced and first-, second-, third-, and fifth-order wave models are described, together with the stream function method.

Chapter 4 is devoted to the wave and current loads on small, or slender, bodies. The Morison equation is introduced and its limitations, in complex wave flows, and in waves and current, are highlighted.

https://doi.org/10.1017/9781009198059.003 Published online by Cambridge University Press

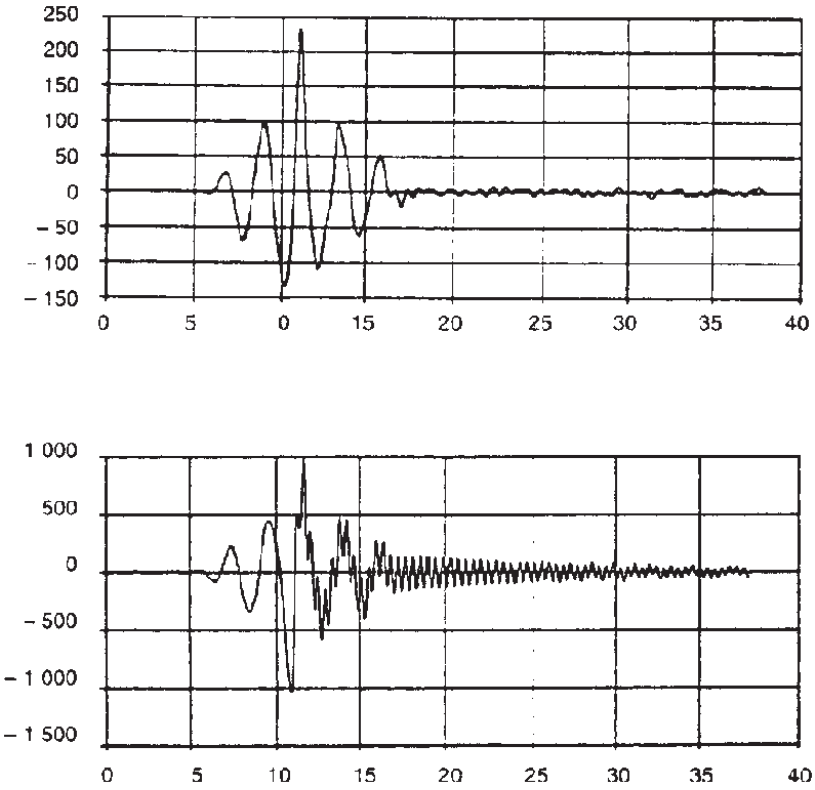

Figure 1.20 Model tests on a vibrating cylinder. Time series of the free surface elevation (top, in mm) and of the bending moment at the foundation (bottom, in m kN).

Chapter 5 addresses hydroelastic instabilities, such as Vortex-Induced Vibrations (VIVs), galloping, flutter, and Wake-Induced Oscillations (WIOs).

Chapters 6–8 are devoted to large bodies, and potential flow theory is applied throughout.

Chapter 6 deals with linear theory. The diffraction-radiation problem is introduced and different techniques of resolution are described. A wide range of applications are proposed, such as wave energy recovery, coupling between sloshing in tanks and sea-keeping, moonpool and gap resonances, etc. Illustrative comparisons with experimental results are presented.

Chapter 7 is devoted to second-order effects: drift forces in regular waves, sum and difference frequency loads in irregular waves, and high- and low-frequency wave responses. The different sources of damping involved in slow-drift motion are identified and tentatively quantified.

Chapter 8 covers some other types of nonlinear loads and responses: ringing loads, third-order runups, parametric instabilities, hydrodynamic impact, and hydrodynamics of perforated structures.

Finally, Chapter 9 covers model testing.

https://doi.org/10.1017/9781009198059.003 Published online by Cambridge University Press

Four appendices follow. The first summarizes the foundations of potential flow theory, the second deals with hydrostatics, the third with damped mass spring oscillators, and the last with the boundary integral equation method.

The reader should have a good background in mathematics and, preferably, in fluid mechanics. For those not acquainted with potential flow theory, the first appendix should be sufficient to provide the basic knowledge.

1.3 References

Etienne S. 1999. Contribution à la modélisation de l'écoulement de fluide visqueux autour de faisceaux de cylindres circulaires, thèse de doctorat de l'université Aix-Marseille II (in French).

Molin B., Bureau G. 1980. A simulation model for the dynamic behavior of tankers moored to single point moorings, in *Proc. Int. Symp. Ocean Eng. Ship Handling*, SSPA.

van Dyke M.D. 1982. *An Album of Fluid Motion*, The Parabolic Press.

https://doi.org/10.1017/9781009198059.003 Published online by Cambridge University Press